Geophysical Prospecting, 2008, **56**, 627–641 doi:10.1111/j.1365-2478.2007.00718.x

Diffraction imaging in depth

T.J. Moser[1]* and C.B. Howard[2]†

[1]*Zeehelden Geoservices, van Alkemadelaan 550A, 2597 AV 's-Gravenhage, The Netherlands, and* [2]*Zeehelden Geoservices, 2e de Riemerstraat 184, 2513 CZ 's-Gravenhage, The Netherlands*

Received October 2007, revision accepted February 2008

ABSTRACT

High resolution imaging is of great value to an interpreter, for instance to enable identification of small scale faults, and to locate formation pinch-out positions. Standard approaches to obtain high-resolution information, such as coherency analysis and structure-oriented filters, derive attributes from stacked, migrated images. Since they are image-driven, these techniques are sensitive to artifacts due to an inadequate migration velocity; in fact the attribute derivation is not based on the physics of wave propagation. Diffracted waves on the other hand have been recognized as physically reliable carriers of high- or even super-resolution structural information. However, high-resolution information, encoded in diffractions, is generally lost during the conventional processing sequence, indeed migration kernels in current migration algorithms are biased against diffractions. We propose here methods for a diffraction-based, data-oriented approach to image resolution. We also demonstrate the different behaviour of diffractions compared to specular reflections and how this can be leveraged to assess characteristics of subsurface features. In this way a rough surface such as a fault plane or unconformity may be distinguishable on a diffraction image and not on a traditional reflection image.

We outline some characteristic properties of diffractions and diffraction imaging, and present two novel approaches to diffraction imaging in the depth domain. The first technique is based on reflection focusing in the depth domain and subsequent filtering of reflections from prestack data. The second technique modifies the migration kernel and consists of a reverse application of stationary-phase migration to suppress contributions from specular reflections to the diffraction image. Both techniques are proposed as a complement to conventional full-wave pre-stack depth migration, and both assume the existence of an accurate migration velocity.

INTRODUCTION

Diffractions are the seismic response of small, but structurally relevant, elements in the subsurface, like small near surface scattering objects, or small scale faults, in general all objects which are small compared to the seismic wavelength. As such, they have a great potential for high-precision interpretation of structural details, and thereby to improve structural imaging and near-surface environmental studies. The high resolution of diffraction images may be, theoretically at least, related to super-resolution, which is the ability to image details beyond the classical Rayleigh limit of half a seismic wavelength.

The importance of diffractions in high-resolution structural imaging has been emphasized in several recent publications (Shtivelman and Keydar 2004; Bansal and Imhof 2005; Grasmueck and Weger 2005; Taner, Fomel and Landa 2006; Fomel, Landa and Taner 2006). This paper may be considered in some respects as a sequel to Khaidukov, Landa and Moser (2004), where many other references can be found. During the review process of Khaidukov *et al.* (2004), and subsequent discussion, it became clear that diffractions have still not made their

*E-mail: mosertj@hotmail.com, t.j.moser@zeehelden.com
†E-mail: c.howard@zeehelden.com

way into mainstream seismic processing and imaging, and that they are still cause for confusion. Therefore a motivation for this paper is to further develop and elaborate on some ideas presented in Khaidukov *et al.* (2004). First of all, we further substantiate the claim that diffractions have been ignored in the conventional processing sequence. We present some simple and elementary examples to illustrate the fact that diffractions are treated as noise in preprocessing, and, more importantly, are disregarded in seismic imaging. In fact, it may be argued that conventional reflection imaging does not even require diffracted waves at all, to obtain coherent images of strong subsurface reflectors. One of the proposals in Khaidukov *et al.* (2004) is to provide the interpreter with two images: the reflectivity image, for interpretation of the main reflectors, and the diffraction image, to fill in the small, but potentially crucial, structural details. We further develop this theme showing how the reflection and diffraction images can be used together for high resolution interpretation.

A second motivation for this paper is to develop diffraction imaging in the depth domain and in the context of a conventional pre-stack depth imaging and migration velocity analysis workflow. The success of imaging diffractions separately from the main wavefield depends on the quality of focusing, which in turn implies an adequate migration velocity has been obtained. Several recent papers in fact use the focusing of diffractions as a criterion for the quality of the migration velocity (Sava, Biondi and Etgen 2004; Fomel *et al.* 2006). Separation of diffractions from the main wavefield in the time domain has the advantage that the focusing can be done ad hoc, that is, for each trace and sample separately, and independently from the velocity model (Khaidukov *et al.* 2004; Taner *et al.* 2006). On the other hand, there are many situations where time imaging is insufficient to obtain an acceptable subsurface image, due to lateral complexities and large velocity contrasts (Biondi 2006). In such situations, depth imaging and depth velocity analysis is warranted, even if the computational cost is higher than for time imaging. In this paper we assume the position that, after all the effort spent in obtaining a good depth image and velocity, it is natural to take an additional step and perform diffraction imaging. This diffraction imaging is then embedded in a pre-stack depth imaging context, and takes full benefit from the accurate velocity already constructed.

We define by 'diffraction imaging' any technique that images diffractions separately, as opposed to the common 'full-wave imaging', which images the full recorded wavefield. We present and further develop two new techniques for diffraction imaging in the depth domain, both of which form a diffraction image by suppressing specular reflections. The first is based on reflection focusing (Timoshin 1978) and justifies the claim made in Khaidukov *et al.* (2004) that by stacking only over the receiver leg of the classical diffraction stack, the stack effectively becomes a reflection stack. The reflection focus panels are then an auxiliary domain, in which reflectivity is focused to points which can be easily identified and used for designing a reflection attenuation filter in the data domain. Diffractions are residuals of that filter and can subsequently be imaged separately to obtain a diffraction image. The second technique applies the fact that the classical migration loop can be subdivided into a part that accounts for specular reflections and a part that does not. By designing an additional weighting function to the migration kernel, which consists in suppressing specular reflections, the migration results in a diffraction image.

The paper is organized as follows. In the first section 'Image resolution and diffractions', we present the relation between diffraction imaging and high- or superresolution. Here, we emphasize the difference between data-driven and image-driven resolution enhancement, and illustrate the inherent limitations of the latter. The second section 'Diffractions and conventional processing' makes the point that diffractions are ignored or treated as noise, in conventional preprocessing as well as migration. In the third section, 'Diffraction imaging techniques in depth', we present the two techniques for diffraction imaging in the depth domain. A section on applications concludes the paper.

IMAGE RESOLUTION AND DIFFRACTIONS

The primary goal of imaging, and diffraction imaging in particular, is to obtain images of subsurface structural elements with maximal sharpness, or resolution. A principal limit to resolution for images obtained from seismic data is posed by the Rayleigh criterion. This criterion gives a minimum to the size of resolvable detail, namely when the images of the details overlap within half a wavelength. It is argued in Khaidukov *et al.* (2004) that super-resolution, or imaging of sub-wavelength size details, is possible under ideal circumstances (and at least in theory), when diffractions are isolated from the main wavefield and imaged separately. The argument is that super-resolution amounts to an extrapolation of the signal outside its frequency band, that this extrapolation is possible when the signal is analytic, and that the signal is analytic when its source function support is limited. In practical situations there are many effects which challenge the possibility of super-resolution, especially the presence of noise, but the argument shows that diffractions, which originate from small

scale scatterers, qualify as the carriers of super-resolution information. If one is interested in reliable high- or superresolution of the image, based on the physics of wave propagation, then diffraction detection and imaging is the key technique.

Nowadays, many techniques exist that aim at enhancing the image resolution and its interpretability. Many of these techniques operate on the image in the post-stack and post-migrated domain, that is after the data gathers have been migrated and stacked (in whichever order). Examples of such image-driven resolution enhancement techniques are coherence analysis (Gersztenkorn and Marfurt 1999; Marfurt *et al*. 1998), instantaneous spectral attributes (Liu and Marfurt 2007), and various structure-oriented filters (e.g., Fehmers and Höckers 2003). Since a seismic image may be thought of as a convolution of a (multidimensional) band-limited wavelet with an infinitely sharp reflectivity distribution, there is some justification for post-stack, post-migration image processing. However, it is important to realize that the scope of image-driven resolution enhancement is limited by the Rayleigh criterion. Moreover, incorrect migration velocities lead to apparent edges in the image, which will be detected as real edges, unless a pre-stack (diffraction) analysis is carried out.

We illustrate this in Fig. 1. Here a simple model consisting of a syncline and a narrow graben is constructed in a constant-velocity background. Figure 1(b) shows a zero-offset section over this model, obtained by Kirchhoff (boundary-integral) modeling. Several phenomena can be distinguished. First, there is the main reflection from the plane interface. Then, there is the wavefront triplication and associated caustic above the syncline. Third, there are the edge diffractions originating from the four edge points in the model. Fourth, there are edge diffractions from the boundaries of the model, due to a finite aperture in the forward modeling. Several events are easily identifiable and interpretable by means of zero-order ray theory: the main reflection and the triplicated branch. Other phenomena are not predictable by standard ray theory: the caustic diffraction at the wavefront triplication, and the edge waves and their kinematic and dynamic behaviour. (It is in fact very illustrative to follow these events also for non-zero offsets but this is beyond the scope of this paper).

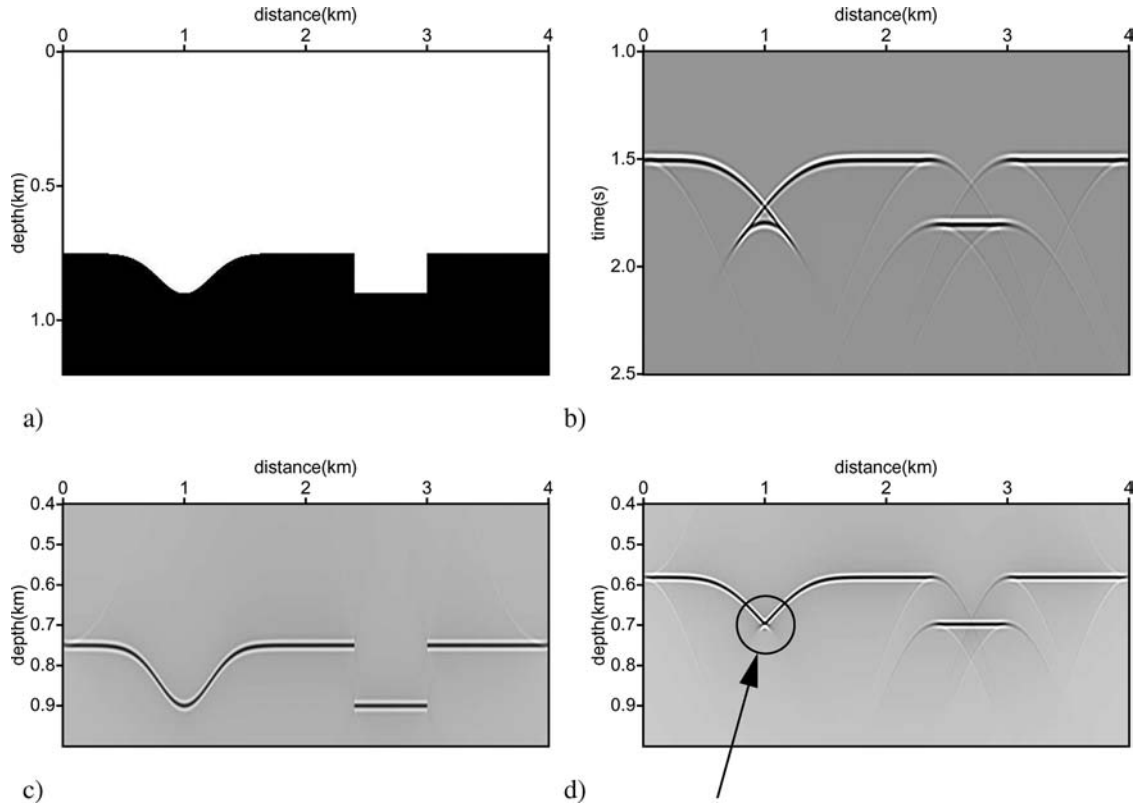

Figure 1 Appearance of migration artifacts. a) model with syncline and simple graben, b) zero-offset section, c) migration using correct velocity, d) migration using a velocity which is too low. A false edge (migration artifact) is indicated by the arrow.

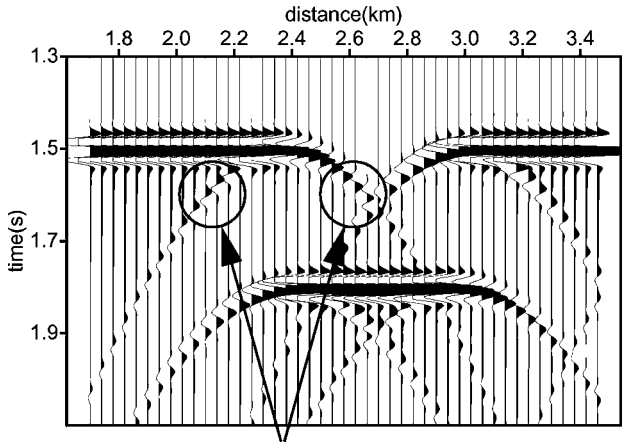

Figure 2 Phase rotation of edge diffracted wave across its apex (indicated by the arrows).

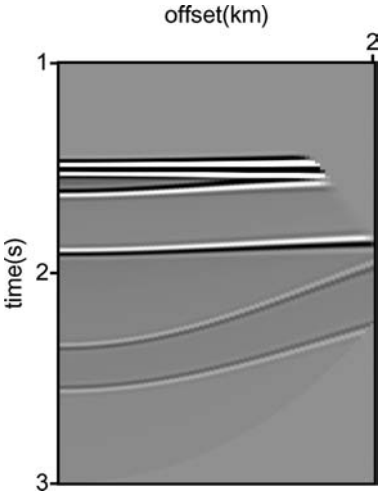

Figure 3 Common data point gather at distance=3.5 km in the model of Fig. 1, after NMO correction with constant velocity. Note that the main reflection has been flattened, but four diffractions, originating from the four edges, are still curved, and hence will be suppressed after stack.

Figure 1(c) shows the migration of the zero-offset section using a correct velocity model, Figure 1d using a velocity that is too low. The image for the correct velocity displays the smooth syncline and has collapsed the edge waves to their corresponding edges. For the image using the incorrect velocity, the edge diffractions are unfocused but still recognizable as diffractions. However, the syncline has collapsed into a focus point, which acts as a breakpoint in the reflector at the trough of the syncline (indicated by the arrow). Any image-driven resolution enhancement algorithm will identify the apparent edge as a real edge and emphasize it (whichever way the algorithm is organized). In summary, spurious edges will be highlighted by post-stack attribute techniques with no real means of determining whether they are real or generated by using an incorrect velocity model.

The main point of diffraction analysis and imaging here is that a false edge can be unmasked as being false, by examining its seismic response in the pre-stack data domain. The seismic response from the syncline (caustic and triplication) is fundamentally different from the response from the edges (edge diffractions). This difference is most apparent in the morphology of the response and its kinematic characteristics. As regards its dynamic characteristics, the amplitude at the focal point or false edge is usually much higher than at the real edges (in fact making it even easier to incorrectly detect it as an edge). As a result, diffractions can be used to distinguish objectively between real edges and migration artifacts.

The difference between diffractive and reflective response goes even beyond kinematics: the edge diffractions exhibit a phase shift of 180° across the diffraction apices (indicated by arrows in Fig. 2). See Klem-Musatov (1994) for details. Until now, the phase rotation of edge diffracted waves across their apices has not been used as a criterion for their separation from the main wave field.

DIFFRACTIONS AND CONVENTIONAL PROCESSING

In this section, we outline the argument that high- or super-resolution information carried by diffractions has been deleted in the final stacked and migrated image - in other words, it is then too late to extract it.

Preprocessing of seismic data, for structural imaging or (reservoir) property estimation, almost always includes a stacking of pre-stack gathers, and hence a kinematical correction of offset-dependent move-out (Normal Move-Out, NMO), with the aim of increasing the signal-to-noise ratio. Elementary geometrical considerations, discussed in great detail in Khaidukov *et al*. (2004), show that the kinematic properties of diffractions are different from those of reflections. The implication is that diffractions have different move-out properties, and are therefore filtered out in the standard NMO and stack procedure, which is geared to stack data along reflection curves. This is illustrated by Fig. 3, which displays a common-midpoint gather in the model of Fig. 1, at the right side of the double-edge system. The gather has been NMO-corrected with the correct constant velocity of the model, so that the main reflection event (top event) is flattened. Despite the use of a correct NMO velocity, however, the diffractions from the four edge points appear as curved events, with a

curvature which is increasing with the distance from the edge points. As a result they are suppressed, or filtered out, in the stacking process. A different approach to preprocessing is therefore needed, if diffractions are to be preserved. One challenge is that they have weak amplitudes, compared to reflections. Another challenge (for edge diffractions) is that they are locally tangent to the reflections from smooth parts of the same reflectors (Taner *et al*. 2006; Fomel *et al*. 2006).

On a more fundamental level, the classical (unweighted) diffraction stack for time or depth migration discriminates against diffractions. This statement has been cause for controversy, because of the very terminology 'diffraction stack' itself. For clarification we invoke Huygens' principle. Huygens' principle for wave propagation defines a new wave front as the envelope of waves emerging from virtual point sources on a previous wave front. The point source waves interfere constructively along the new wave front, and destructively elsewhere. Huygens' principle is equally valid for reflected waves (envelopes of elementary diffractions) and for edge diffractions. However, this distinction between *elementary* and *real* diffractions has long been overlooked in seismic imaging. The elementary diffractions are mathematical idealizations that together make up reflections from smooth reflectors, and are, as such, not individually observable. Real diffractions originate from edges or small scattering objects, and are observable on a seismic section. The classical diffraction stack is based on the fact that, in the data domain, a reflection is the envelope of elementary diffractions, and in the image domain, a reflector is composed of elementary diffractors. The classical diffraction stack may take both elementary and real diffractions as input, but the envelope mechanism works only for the elementary ones. It is a correct statement, therefore, that reflector imaging does not need any real diffractions, as defined above in this section. Another correct statement is that real diffractions are lost in the classical diffraction stack (again, despite its name), and that the latter is biased towards reflections. Of course, in special migration designs like the stationary-phase migration (Schleicher *et al*. 1997; Chen 2004), the bias against diffractions is even more explicit.

Figure 4 offers an illustration. In Fig. 4(b) a reflector is drawn, with two end points, and a very small fault in the middle. Figure 4(a) is a zero-offset section over this model. The main reflection is clearly visible, as well as edge diffractions from the two end points and from the central microfault. In fact, Figures 4(a) and 4(b) can be considered as migrated and demigrated versions of each other. If we reduce the number of scatter points along the reflector (Fig. 4d), then from the associated zero-offset section (Fig. 4c) it becomes clear, that the reflection is composed of elementary diffractions. These elementary diffractions are indeed invisible in the original reflection (Fig. 4a), which is their envelope. If we are able to extract the real diffractions from the full wavefield, and image them separately, we have diffraction imaging. This is illustrated by the bottom plots of Fig. 4: in Fig. 4(e) the real edge diffractions, in Fig. 4(f) the image of the diffracting edges.

DIFFRACTION IMAGING TECHNIQUES IN DEPTH

There are several motivations to study diffractions in the depth domain. The appearance of diffractions in the seismic data is usually evidence for strong complexities and a strongly inhomogeneous trend model. Such complexities can invalidate the assumptions of time migration (local lateral homogeneity), so that pre-stack depth imaging is then the method of choice. Pre-stack depth imaging is more labour and compute intensive than time imaging, due to the migration velocity analysis and the computation of travel time tables. On the other hand, the success of identifying and isolating diffractions depends on the quality of focusing or the accuracy of the velocity model. It is therefore a natural step to complement the full-wave pre-stack depth imaging with a diffraction analysis and -imaging step, where full benefit is taken from the already constructed velocity model. If the velocity model is accurate and detailed enough for an optimally focused full-wave depth image, then for the diffraction image no additional focusing is needed.

In this section, we present two techniques for diffraction imaging in the depth domain: reflection focusing and the anti-stationary phase filter. Both approaches are tested and illustrated on the Cassis data set (provided by Total/Opera, Pau). This is a Marmousi-like model with channel structures in the deeper sections, embedded in a set of horizontal plane reflectors. For comparison, reference and the ease of exposition of the diffraction imaging techniques, we first present a full-wave pre-stack depth imaging (Figs 5 and 6). A conventional full-wave Kirchhoff migration (Hubral, Schleicher and Tygel 1996) applies the classical diffraction stack

$$V(\mathbf{x}) = \int \mathrm{d}t\ \mathrm{ds}\ \mathrm{dr}\ w(\mathbf{s},\mathbf{x},\mathbf{r})\ U(t,\mathbf{s},\mathbf{r})\ \delta(t - t_d(\mathbf{s},\mathbf{x},\mathbf{r})), \qquad (1)$$

and uses a stacking travel-time trajectory given by

$$t_d(\mathbf{s},\mathbf{x},\mathbf{r}) = T(\mathbf{s},\mathbf{x}) + T(\mathbf{x},\mathbf{r}), \qquad (2)$$

where $U(t,\mathbf{s},\mathbf{r})$ are the full-wave data, depending on time t and shot/receiver position **s**/**r**, and δ the Dirac delta function. The

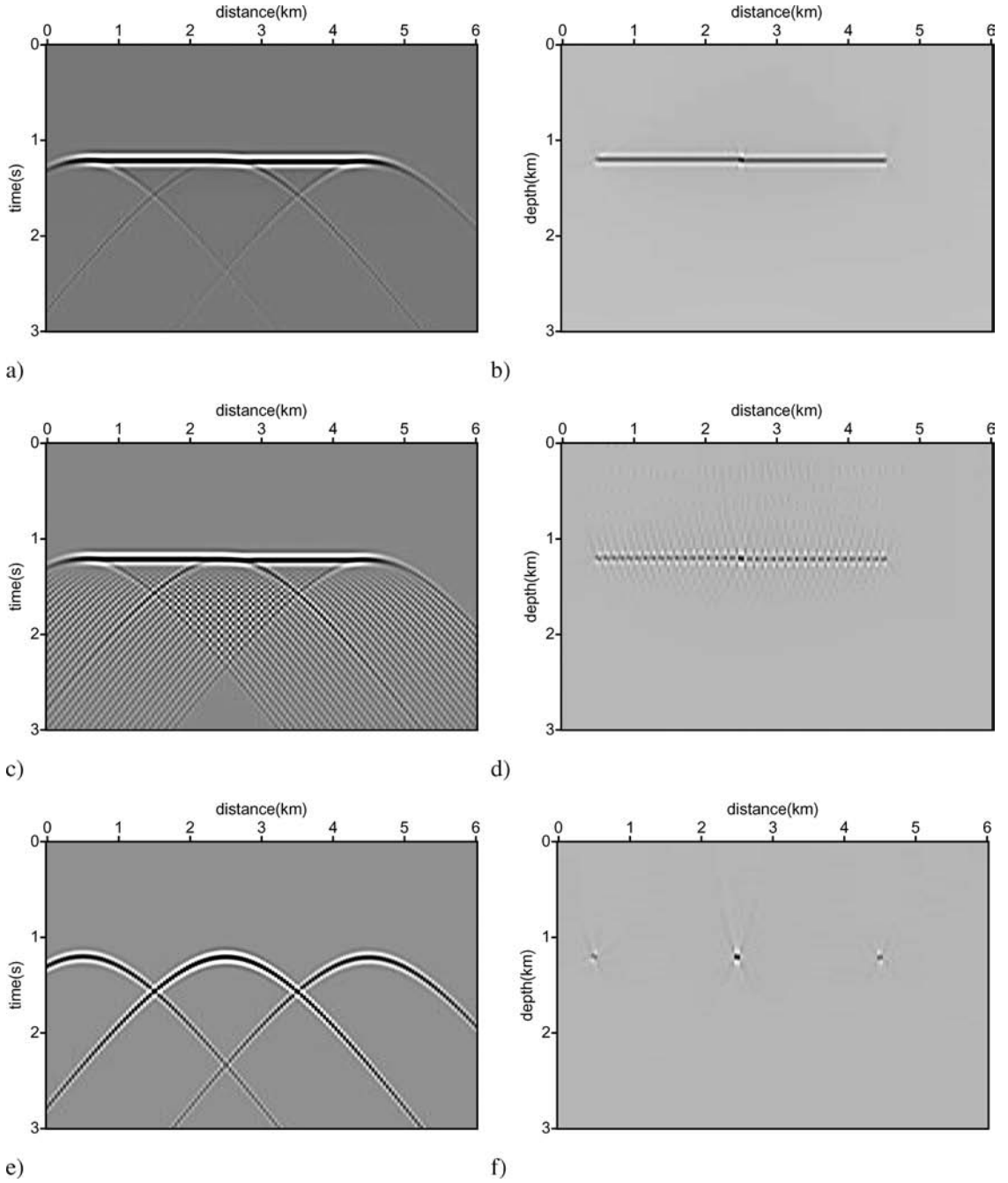

Figure 4 a) zero-offset section over a plane reflector segment with a small fault. Note diffractions from the fault and the edges of the reflector. c) decomposition of zero-offset into edge diffractions and a finite number of elementary diffractions. e) edge diffractions. b), d), f) migrated image of the data in the left panels.

reflectivity image is given by $V(\mathbf{x})$, depending on the subsurface image point $\mathbf{x}$. The weighting function $w(\mathbf{s}, \mathbf{x}, \mathbf{r})$ is chosen equal to one here. The stacking travel-time trajectory $t_d(\mathbf{s}, \mathbf{x}, \mathbf{r})$ represents the travel time of an *elementary* diffraction from the image point $\mathbf{x}$, and plays a crucial role in the envelope mechanism, described in the section 'Diffractions and conventional processing'. $T(\mathbf{s}, \mathbf{x})$ is the travel time from $\mathbf{s}$ to $\mathbf{x}$ (and similarly for $T(\mathbf{x}, \mathbf{r})$), which may be multivalued in case of multipathing. For a sufficiently dense grid covering the source-receiver acquisition, the travel times are pre-computed by ray

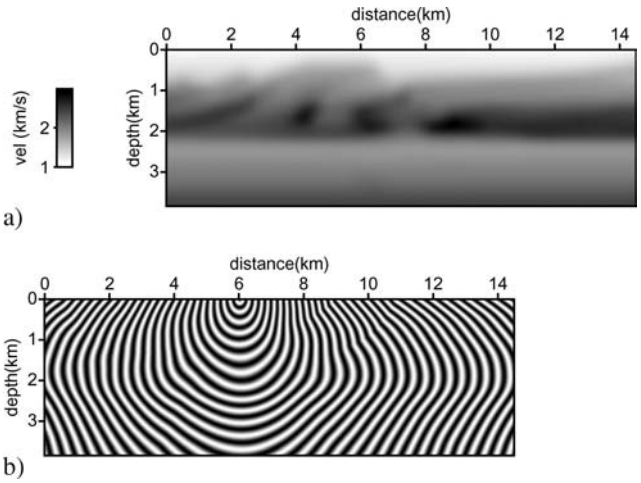

Figure 5 a) migration velocity model for the Cassis data set. b) traveltimes from a location at distance = 6 km (grey scale representing cos 50 t, t in seconds).

tracing in the background velocity model, and stored on disk as travel-time tables for subsequent use in the diffraction stack (1). This process is summarized in Figs 5 and 6, displaying the velocity model (Fig. 5a), an exemplary travel-time table (Fig. 5b), and the final pre-stack depth migrated image (Fig. 6), using the full-wave data.

Removing specular reflections by reflection focusing

Reflection focusing (Timoshin 1978; Khaidukov *et al*. 2004) uses the fact that a reflection travel-time curve can be regarded as a diffraction travel-time curve, for a virtual source mirrored on the opposite side of the reflector. Stacking the seismic data over the reflection curve, given by

$$t_r(\mathbf{s}, \mathbf{x}, \mathbf{r}) = T(\mathbf{x}, \mathbf{r}), \tag{3}$$

that is, replacing t_d (2) by t_r (3) in the stack (1), allows to focus reflected energy to its virtual source point. This virtual source point is typically located twice as deep as the reflector (see Fig. 7). In this way, each shot gather from the pre-stack data can be transformed in a reflection-focus gather. Reflections can be identified in the reflection-focus gather as points with sharply focused energy, which can be found by a simple scanning algorithm. These reflection focus points can be used to construct diffraction shot gathers, where the reflections have been removed or suppressed, in basically two ways (Khaidukov *et al*. 2004). One way is to mute the reflection focus points and to demigrate the residual energy (using the same reflection travel times t_r (3)). The other way, followed here, is to use the reflection focus points to design a suppression filter in the corresponding shot gather, again using the same reflection travel times. The reflection focus points, together with the reflection travel times, define travel-time trajectories of reflection events. Along these trajectories, a moving window median filter is applied to remove the reflected energy. The residual of that filter is a diffraction shot gather. As a last step, the diffraction gathers are input to the normal classical diffraction stack (1) with travel times given by (2). Since after successful filtering the diffraction gathers are supposed to contain only *real* diffractions and no more *elementary* ones, the envelope mechanism does not play a role,

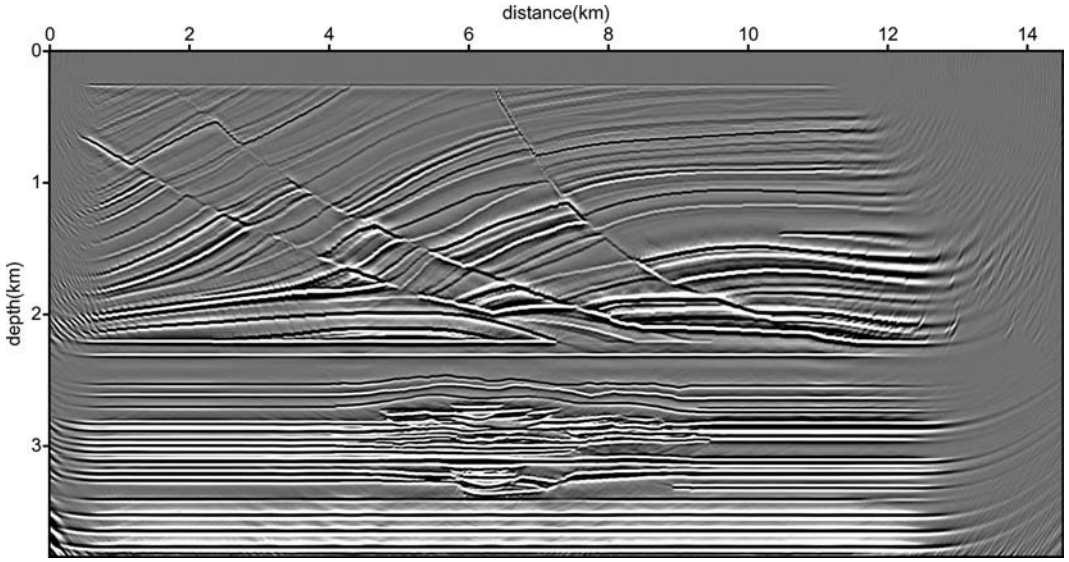

Figure 6 Full-wave prestack-depth migration image.

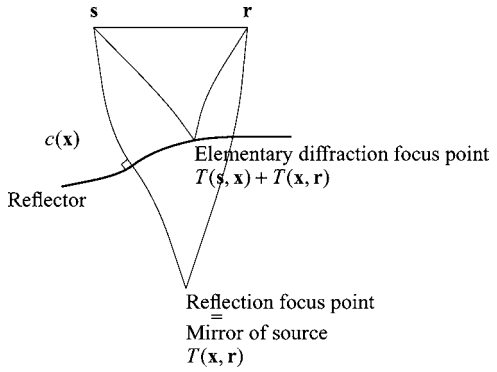

Figure 7 Geometry of reflection focusing. The reflection on the displayed reflector is focused to its own focus point, and is kinematically equivalent to a point diffraction from that point.

and each real diffraction is stacked and imaged to its own diffractor.

We make several comments to this procedure. First, the reflection focusing was proposed in Khaidukov *et al.* (2004) for application in a macro-model independent context. Here we demonstrate that the procedure also works when using an available depth velocity model and using the reflection curve (3). Second, it is an interesting question which velocity is needed at the mirror side of the reflector, to make sure that the reflection is focused in one point. For shallow reflectors, we may take the existing deeper parts of the velocity model, for deep reflectors, the velocity model will have to be extrapolated to (about) twice its original depth range. Third, the reflection will strictly focus to a point only in simple cases like a constant velocity above a plane reflector. Generally, a reflection will focus to a curved line segment that acts as a caustic (the shape of the caustic depends on parameters such as receiver offset range, model complexity, reflector curvature, and the velocity continuation beneath the reflector). Another smearing effect is caused by the finite aperture of the acquisition. In any case, both effects can be accounted for by adjusting design parameters in the focus scanning algorithm and the subsequent median filtering (or, alternatively the muting and defocusing).

The procedure for removing specular reflections by reflection focusing is illustrated on the Cassis data set in Figs 8 and 9. In Fig. 8(a) a single full-wave shot gather (at shot location 1.1km) is displayed, with a typical strong reflection highlighted by the ellipse. For reference, a partial Kirchhoff migration of this gather is shown in Fig. 8(b). This image is obtained by applying the diffraction stack (1) with the stacking trajectory (2) for the fixed source point. Figure 8(d) displays the reflection focus gather for the same source point, obtained by applying (1) with the stacking trajectory (3). In this image, the reflections are focused to sharp localized caustics. The maxima of these caustics are localized by the scanning algorithm, consisting of a moving window, where the absolute energy of the midpoint is checked against the absolute energy in all other points of the window. For maxima found by this scanning, the corresponding reflections in Figure 8a are filtered out by the moving window median filter. The resulting diffraction shot gather is displayed in Fig. 8(c) (note that the flow of computations follows Figs 8a $\rightarrow$ 8d $\rightarrow$ 8c). Comparison with Fig. 8(a) shows that important reflections, for example the one highlighted by the ellipse, have been removed or suppressed. Repeating this for all shot gathers, and inserting the resulting diffraction shot gathers into the diffraction stack (1), with the normal stacking trajectory (2), yields the diffraction image displayed in Fig. 9. We note that we have not attempted the focusing of deeper reflections in these tests. As a result, the deeper reflections (below 2km depth) have not been filtered out in Fig. 9. For the upper part of the section however (above 2km depth), the reflection energy has been suppressed and the diffractors stand out.

Removing specular reflections using an anti-stationary phase filter

Stationary-phase migration (Bleistein 1987; Schleicher *et al.* 1997; Chen 2004) aims at emphasizing contributions to the migrated image from specular ray reflections. The main objective is to reduce aliasing effects in the migrated image. Emphasizing specular ray reflections is done by limiting the migration aperture to the Fresnel zone around the specular reflection point. This can be implemented by the weight function $w(\mathbf{s}, \mathbf{x}, \mathbf{r})$ in the classical diffraction stack (1). For given ray vectors $\mathbf{p}_s = \nabla_x T(\mathbf{s}, \mathbf{x})$ and $\mathbf{p}_r = \nabla_x T(\mathbf{r}, \mathbf{x})$ from the source and receiver, respectively, and a local unit normal vector to the reflector $\mathbf{n}$, the weight function can be designed as follows:

$$w(\mathbf{s}, \mathbf{x}, \mathbf{r}) = \mathbf{n}^T(\mathbf{p}_s + \mathbf{p}_r)/||\mathbf{p}_s + \mathbf{p}_r||. \quad (4)$$

which is the inner product of the reflector unit normal and the bisectrix of the in- and outgoing ray vectors at $\mathbf{x}$. The weighting function defined by (4) attains its maximum when the reflector normal and the bisectrix are collinear, which is precisely the case of specular ray reflection. The Fresnel zone around the specular reflection point can be defined as $w(\mathbf{x}, \mathbf{s}, \mathbf{r}) > 1 - \varepsilon$, where ε is a small number, which is frequency dependent. This is illustrated in Fig. 10 (above).

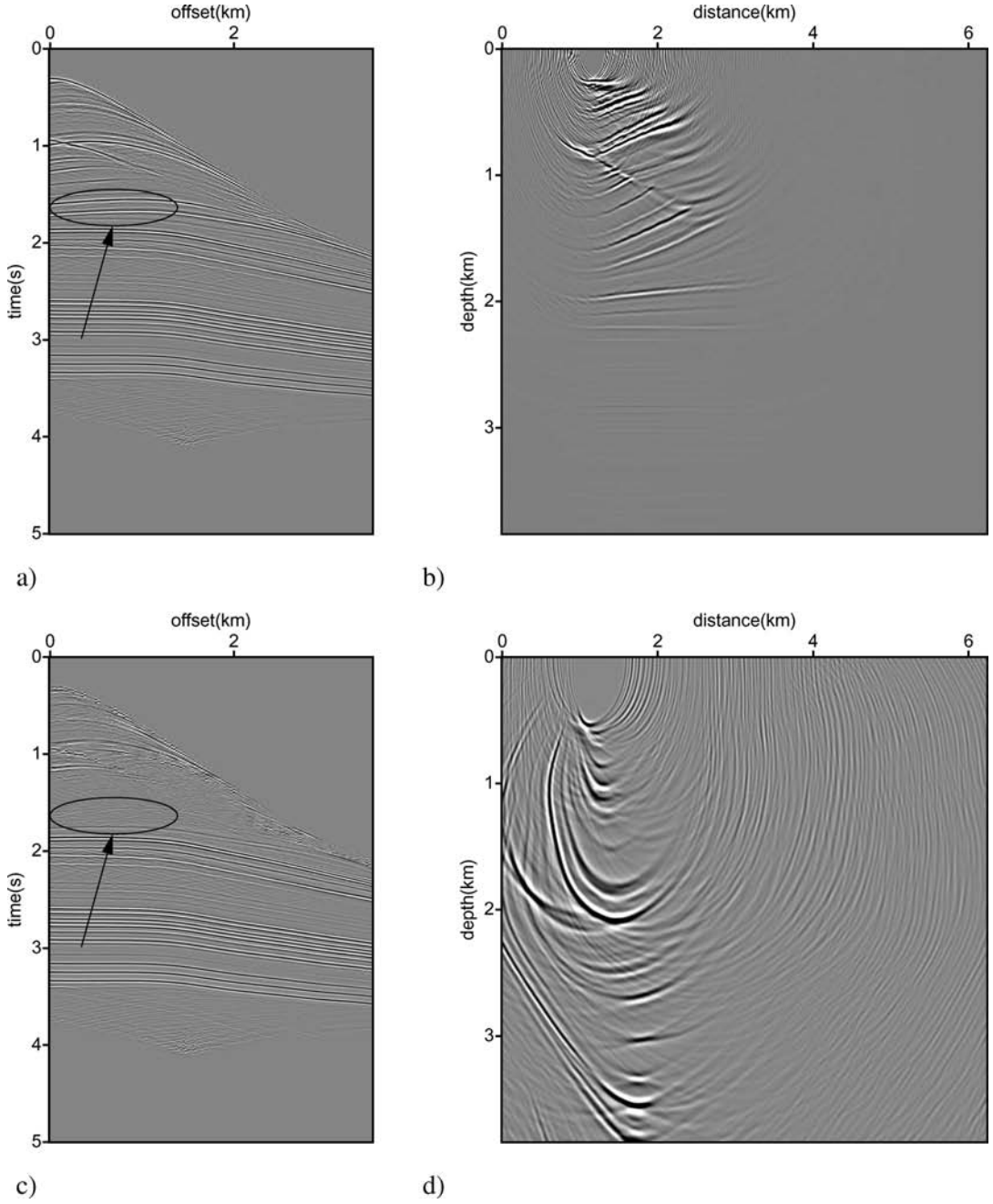

Figure 8 Reflection focusing on one shot gather from the Cassis data (at shot location 1.1 km). a) original gather, b) depth migrated with the full stacking curve given by equation (2). c) diffraction shot gather, obtained by identifying maximum reflection points in the reflection focus gather (Fig. 8d), and using them to filter out reflections in the original shot gather. The ellipse indicated by the arrow highlights a reflected wave which is suppressed after the filtering. d) reflection focus gather, obtained by depth migrating the original shot gather (Fig. 8a) with the stacking curve given by equation (3).

Diffraction imaging by anti-stationary phase filtering does precisely the opposite (Kozlov *et al*. 2004). Here, the weighting function is constructed to suppress specular reflections:

$$w(\mathbf{s}, \mathbf{x}, \mathbf{r}) = 1 - \mathbf{n}^T(\mathbf{p}_s + \mathbf{p}_r)/||\mathbf{p}_s + \mathbf{p}_r||, \quad (5)$$

so that it vanishes for the case of collinear reflector normal and bisectrix of in- and outgoing ray vectors at $\mathbf{x}$. By this design, non-specular reflections (or diffractions) are enhanced in the classical diffraction stack. These are the ray paths hitting the reflector outside the Fresnel zone (Fig. 10, below). We

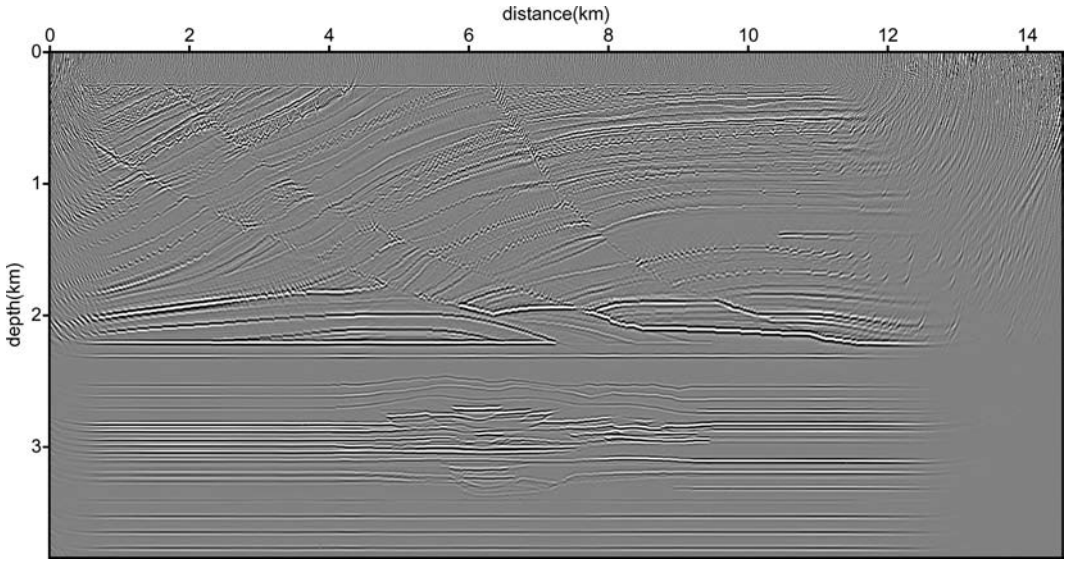

Figure 9 Diffracted wave prestack-depth migration image, using diffraction shot gathers obtained by reflection focusing and filtering (see Fig. 8). Note that the reflectors in the bottom half of the image have not been suppressed, because the algorithm was applied here using only the available depth velocity model (Fig. 5a), without the required extrapolation to twice the depth range.

refer to the weight function (5) as the *anti-stationary phase filter*.

Some implementation details of diffraction imaging by anti-stationary phase filtering are as follows. First, a reflector dip field needs to be constructed for each image point **x**. There are several approaches to obtain reflector dips from a full-wave image (Tygel *et al*. 1993; Fomel 2002; Marfurt 2006). Here, we apply a simple approach of a local slant stack, by searching for a local plane segment through **x** with maximal semblance in the full-wave image. Second, the ray vectors $\mathbf{p}_s$ and $\mathbf{p}_r$ can be obtained by differentiating the corresponding travel-time fields, or by paraxial ray tracing. Third, the weight function (5) is moderated by a monotonic gain function (i.e. a power gain), which controls the amount of reflectivity to be suppressed. For simplicity, it is assumed that **n** and $-\mathbf{n}$ represent the same reflector dip, by taking the absolute value (or an even power) of the inner product in (5). Finally, the classical diffraction stack (1) is carried out with full-wave data as input, but with the moderated weight function.

We illustrate the procedure of removing specular reflections by reflection focusing on the Cassis data set in Figs 11 and 12. Figure 11 shows the horizontal and vertical components of the reflector normal field (representing the dip), obtained from the full-wave pre-stack depth migrated image of Fig. 6, by the local slant-stack procedure (which consists of finding, at each image point, the dip with maximum semblance over a local plane segment among a relevant range of dips). Since most reflectors are horizontally oriented, the horizontal reflector normal component is close to zero, and the vertical component close to one; at the reflector and fault junctions, the normals are variable and less well defined (lower maximum semblance). Figure 12 shows the diffraction image, obtained by applying the diffraction stack (1) with the conventional stacking trajectories (2), but the modified migration kernel, given by equation (5). Note that reflector energy has been removed or suppressed here over the full depth range of the image, with some residuals remaining in the deeper part (due to fixed filter settings over the depth range).

Sensitivity to velocity errors

The main argument of this paper is that as soon as a high-quality full-wave pre-stack depth migration and corresponding migration velocity analysis have been completed, the same velocity information can be used advantageously for diffraction imaging. However, the implications of an erroneous velocity on diffraction imaging remain an important issue. One question is whether the diffraction image is as sensitive to velocity errors as the full-wave image. Another question is which phenomenon is likely to occur first, when the velocity becomes increasingly erroneous: the appearance of migration artifacts for full-wave imaging, illustrated and discussed in Fig. 1(d), or the defocusing of diffracted images. If diffracted images can be shown to be stable and detectable for a significant range of velocity deviations, that would argue in favor of diffraction imaging. In any case, a migration artifact due to an

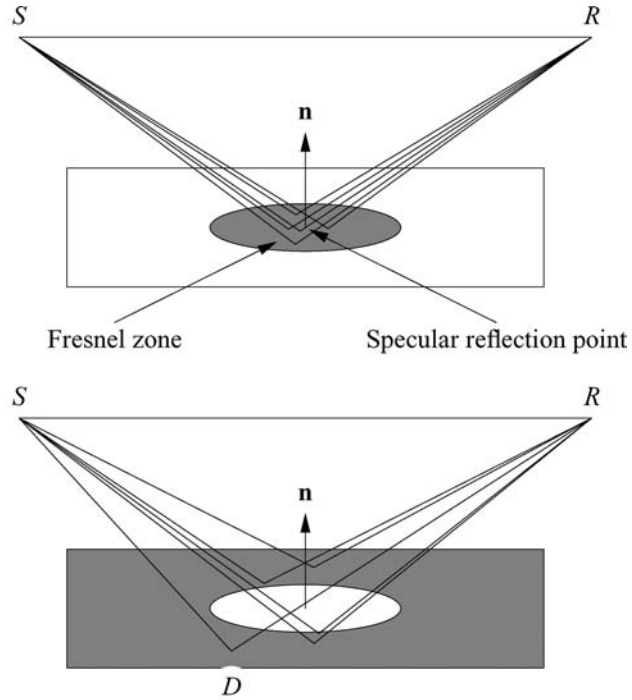

$$\frac{1}{2}(SD + RD).\mathbf{n} < 1 - \varepsilon$$

Figure 10 Schematic illustration of the principle of anti-stationary phase filtering. Top: conventional stationary phase migration uses only (specular) reflections within a Fresnel zone around the reflection point. Bottom: diffraction imaging using the anti-stationary phase filter uses only non-specular responses from the reflector outside the Fresnel zone.

erroneously focused syncline can be distinguished from a defocused diffracting edge (Fig. 1d, at distance 1 km and 2–3 km, respectively) by using additional amplitude and phase property information of diffractions (as we point out at the end of the section 'Image resolution and diffractions'). Additionally, if common-image gathers are constructed for diffraction imaging (the same way they are constructed for full-wave imaging), then a defocused diffractor image will appear with a certain move-out; a diffraction residual move-out may then improve the focusing.

To examine the effect of an erroneous velocity on diffraction imaging, we show in Fig. 13 the results of the reflection-focusing technique (where velocity is more critical than in the anti-stationary phase technique) with three different velocities: the correct velocity, a 10% too low, and a 10% too high velocity. As expected, for the too low velocity the image is shifted downward and the diffractors become smiles, for the too high velocity they become frowns. In both cases, the reflectors are less well attenuated, but still the diffractors can be clearly distinguished.

APPLICATIONS

Diffraction imaging has a wide range of applications and potential applications: ground-penetrating radar (GPR) imaging (Grasmueck and Weger 2005), environmental studies (Shtivelman and Keydar 2004), archeology, and others. We elaborate here in some detail on the potential of using diffractions in high-quality reservoir imaging. Small scale faults may affect reservoir flow properties very strongly and so identifying and positioning these may be critical in developing a representative reservoir model and hence to the chosen development scenario. Since the identification of small scale fractures on reflection seismic generally depends upon identifying bedding displacements (fault surfaces are generally poor reflectors for a standard acquisition geometry), we can only see fractures where the seismic resolution allows. Faults with small displacement or joints may not be resolved, and tracing a fault as the throw decreases, for example when it enters a relay zone, may be unreliable. Diffraction imaging attempts to remove the specular reflections arising from the bedding planes and leaves only the diffractions arising from the rough fault surfaces or from within fault zones. The magnitude of these diffractions is not controlled by fault displacement, but more by the roughness of the fault surface and the contrast of impedance between the fault zone content and the surrounding beds. This implies that we could theoretically trace a fracture even when there is zero displacement (that is, beyond Rayleigh's resolution criterion). Constructing a static model of a (faulted) reservoir usually starts with building a fault framework and then, when this is complete, attaching the bedding geometry. The diffraction image will be useful to help build this fault framework, perhaps as a combined display with the reflection image, resulting in a fault model with better defined fault planes and fault zones, even when fault displacements are low. Also, fractures due to differential stress, on the crest of an anticline for example, would be more easily identified using diffraction imaging. Stratigraphic traps rely on the position of pinch-outs of sediment geometries either due to a facies change or an erosional truncation. Because of the resolution of seismic data, to assign the position of a pinch-out the interpreter has to extrapolate an interpretation of two bedding surfaces (or one bedding and one erosional surface) until they intersect. Because of the low angles, and the inherently rough nature of geological bedding surfaces, the position error may be very large. Diffraction imaging could be used

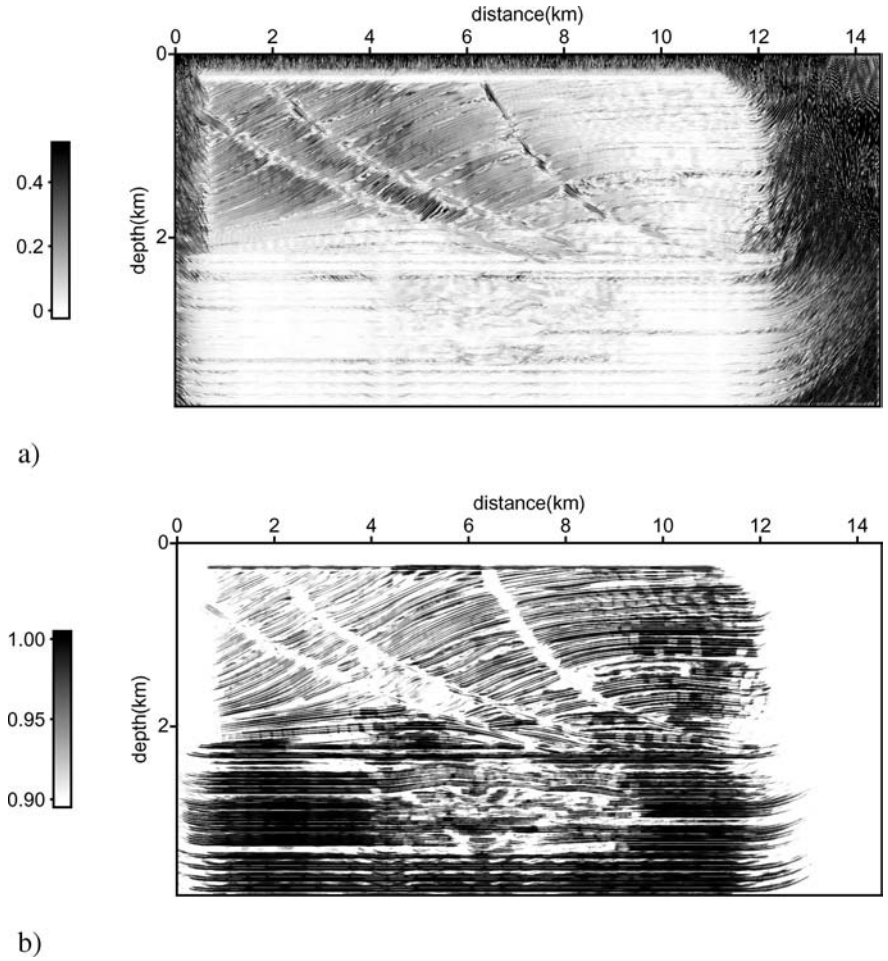

Figure 11 Dip field obtained from the full-wave prestack-depth migration image by a local slant-stack approach: a) horizontal component of reflector normal, b) vertical component.

to identify changes in roughness of an interface, and hence indicate the positions of pinch-outs and construct sub-crop maps at unconformities.

As an illustration, we highlight a few features in the diffraction image of Fig. 12. First, pinch-outs are imaged very sharply at several locations. Figure 14(a) shows a zoom on a pinch-out at distance 2.3 km and depth 2.2 km. In the full-wave image it is hardly distinguishable and very difficult to localize. By contrast, in the diffraction image it is easily detectable as the last diffraction cross along the upper pinching reflector. In fact, one may be tempted to label this case as superresolution imaging, at least indirectly. The location of the pinch-out constitutes information that is not available in the full-wave image, because of the overlapping of the band-limited images of the two reflectors approaching each other (from right to left). The fact that the diffraction image does allow to accurately locate the pinch-out would imply imaging to sub-wavelength scale, and therefore beyond the Rayleigh limit. Figure 14(b) shows a zoom on the main fault system from distance 6.5 km to 8 km. Here the fault junctions with the horizontally oriented reflectors are much more prominent in the diffraction image than in the full-wave image. The third example, displayed in Fig. 14(c), illustrates diffraction imaging on so-called rough horizons, i.e., reflectors with many small-scale discontinuities and other diffracting elements. In this case, the discontinuities are caused by a grid representation of the velocity model used in generating the synthetic data. Nevertheless, the fact that these grid edges are accurately imaged in the diffraction image shows the power of the diffraction imaging method (even to the extent that the grid diffractors can be counted and the original grid size may be reconstructed). Phase characteristics of the imaged diffractors provide additional structural information on the orientation of the small-scale discontinuities and the sign of the impedance contrasts.

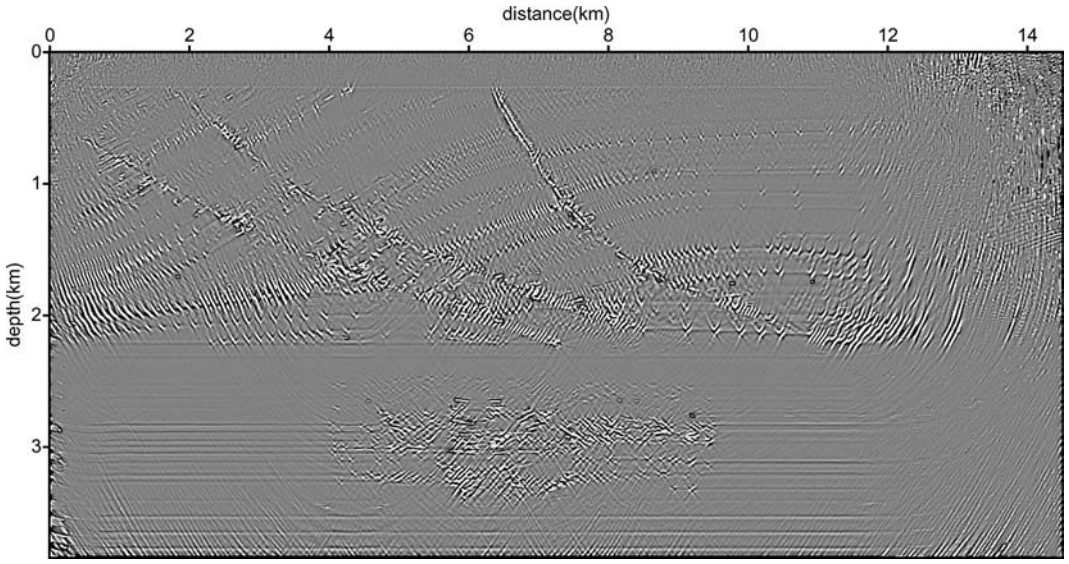

Figure 12 Diffracted wave prestack-depth migration image, obtained by anti-stationary phase filtering.

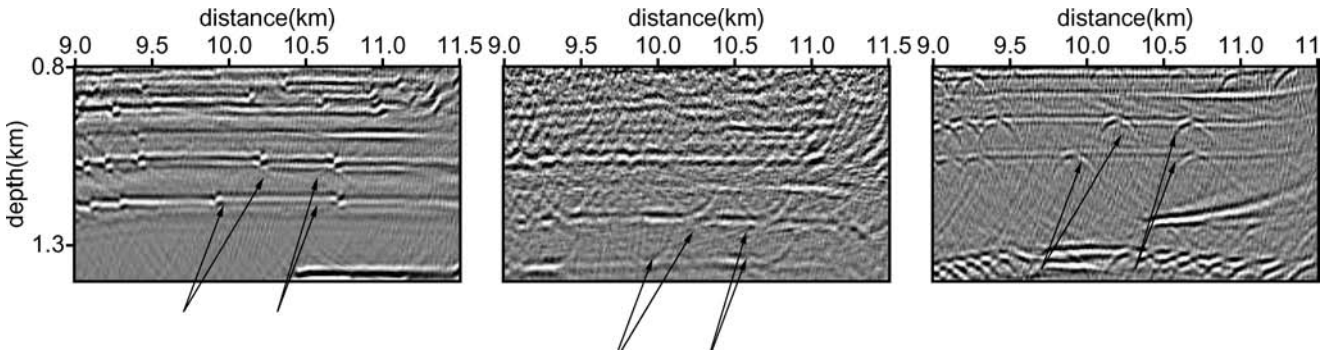

Figure 13 Sensitivity of diffraction image on velocity errors. Zoom on Figure 9 (diffraction image by reflection focusing). Left to right: diffraction image with correct velocity, 10% too low velocity, 10% too high velocity. Note reflectors are less attenuated for erroneous velocities, diffractors are still distinguishable.

DISCUSSION AND CONCLUSIONS

Reliable and physically meaningful extraction of high- or even superresolution attributes from a seismic image requires analysis and imaging of diffracted waves. Since diffractions are treated as noise in conventional processing, they are best analyzed (identified, filtered, separated from the full-wave field) in the pre-stack domain. Even conventional imaging using the classical diffraction stack treats real diffractions unfavorably, so they need to be imaged separately from the full-wave field. The result is then a diffraction image, which can be used as a complement to the conventional reflection image, and is of great help to an interpreter.

Techniques for diffraction analysis require proper focusing. Hence, they are especially suitable to be combined with pre-stack depth imaging and migration velocity analysis. Since these are compute intensive and time consuming processes, the obvious question arises: why not to take another step, and use the accurate depth velocity model (and traveltime tables) to construct a diffraction image?

We present and further develop two techniques for diffraction imaging in the depth domain, in the framework of a completed pre-stack depth imaging and migration velocity analysis process. First, we show that reflection focusing in the depth domain by means of stacking only over the receiver leg of the classical diffraction stack indeed works (as anticipated by Khaidukov *et al*. 2004). The reflection focus points can be easily detected by a scanning algorithm and used to define reflection suppression filters on the full-wave shot gathers. The residuals of these filters are diffraction shot gathers,

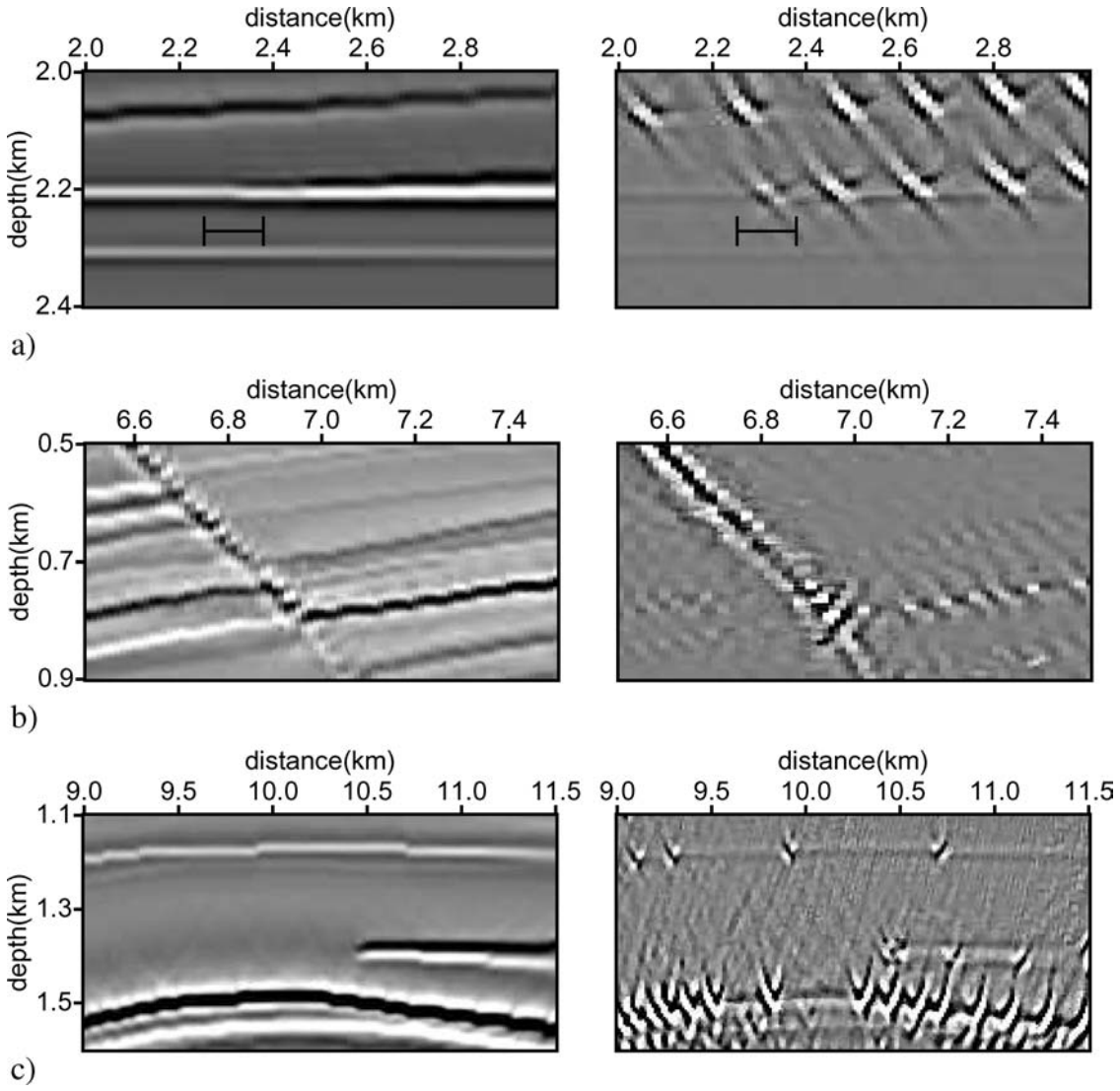

Figure 14 Examples of diffraction imaging. Left column: zooms on full-wave image of Fig. 6; right column: zooms on Fig. 12 (diffraction image by anti-stationary phase filtering). a) pinch-out example. Pinch-out indicated by the "H"-symbol. Note that the diffraction image allows a very precise localization of the pinch-out being the last diffraction along the pinching reflector. Since this degree of detail is lost in the full-wave image we may speak of (indirect) superresolution. b) fault example. The fault stands more out in the diffraction image. c) rough horizon example. Here the rough horizon is imaged properly in the full-wave image, but its roughness is much easier to interpret in the diffraction image. Also note phase rotations (in black and white) in the diffraction image, corresponding to the impedance contrast across the diffractors.

and diffraction imaging consists in imaging them separately from the full-wave. Diffraction imaging by reflection focusing requires a velocity model with a much larger depth range than the full-wave imaging, typically twice as deep. The second method reverses the stationary-phase principle to enhance diffractions (non-specular scattering) and suppress reflections (specular scattering). This method requires a reflector dip field to be extracted from the full-wave image. By modifying the weighting function in the migration kernel in such a way that specular ray reflections are suppressed, or, equivalently, all scattering within the first Fresnel zone, we obtain an anti-stationary phase filter. Diffraction imaging by anti-stationary phase filtering consists then in applying the classical diffraction stack with the modified migration kernel.

We note that for both methods we assume a sufficiently accurate velocity model, that is, a model which is sufficient to enable an optimally focused full-wave pre-stack depth image. We do not discuss in this paper any mechanism for additional

focusing. As such, the methods presented here do not themselves allow to unmask the migration artifacts, which are the result of an inadequate migration depth velocity model. Such artifacts need to be analyzed by additional pre-stack diffraction analysis tools. However, the pre-stack depth diffraction imaging allows to construct common-image gathers, where residual move-out may be used to improve the diffraction focusing. Such diffraction residual move-out analysis is a topic of ongoing research.

We did not investigate the effect on diffraction imaging of a low signal-to-noise ratio in the pre-stack data. A high noise level compromises the quality of the reflection suppression filtering based on reflection focusing, and also the extraction of a reflector dip field for anti-stationary phase filtering. We would expect noise to be equally detrimental to both diffraction imaging processes as it is to full-wave pre-stack imaging.

Diffraction imaging can be of great help to an interpreter. Many structural features, such as small-scale faults and pinchouts, are much easier to localize, identify and characterize on the diffraction images. In several such cases, we may be even tempted to label the images as superresolution images. We intend to carry out a number of case studies on real production data to further the case of diffraction imaging.

ACKNOWLEDGEMENTS

The authors appreciate discussions with Evgeny Landa and Shmoriahu Keydar. We are also grateful to Opera (Pau), for making the 'Cassis' data set available for tests.

REFERENCES

Bansal R. and Imhof M.G. 2005. Diffraction enhancement in prestack seismic data. *Geophysics* **70**, V73–V79.

Biondi B. 2006. *3D Seismic Imaging*. SEG, Investigations in Geophysics, 14.

Bleistein N. 1987. On the imaging of reflectors in the earth. *Geophysics* **52**, 931–942.

Chen J. 2004. Specular ray parameter extraction and stationary-phase migration. *Geophysics* **69**, 249–265.

Fehmers G.C. and Höckers C. 2003. Fast structural interpretation with structure-oriented filtering. *Geophysics* **68**, 1286–1293.

Fomel S. 2002. Applications of plane-wave destruction filters. *Geophysics* **67**, 1946–1960.

Fomel S., Landa E. and Taner M.T. 2006. Post-stack velocity analysis by separation and imaging of seismic diffractions, 76th SEG meeting, New Orleans, Louisiana, USA, Expanded Abstracts, 2559–2563.

Gersztenkorn A. and Marfurt K.J. 1999. Eigenstructure-based coherence computations as an aid to 3-D structural and stratigraphic mapping. *Geophysics* **64**, 1468–1479.

Grasmueck M. and Weger R. 2005. Full-resolution 3D GPR imaging. *Geophysics* **70**, K12–K19.

Hubral P., Schleicher J. and Tygel M. 1996. A unified approach to 3-D seismic reflection imaging, Part I: Basic concepts. *Geophysics* **61**, 742–758.

Khaidukov V., Landa E. and Moser T.J. 2004. Diffraction imaging by focusing-defocusing: An outlook on seismic superresolution. *Geophysics* **69**, 1478–1490.

Klem-Musatov K. 1994. *Theory of Seismic Diffractions*. SEG, Tulsa.

Kozlov E., Barasky N., Koroloev E., Antonenko A. and Koshchuk E. 2004. Imaging scattering objects masked by specular reflections, 74th SEG meeting, Denver, Colorado, USA, Expanded Abstracts, 1131–1135.

Liu J. and Marfurt K.J. 2007. Instantaneous spectral attributes to detect channels. *Geophysics* **72**, P23–P31.

Marfurt K.J. 2006. Robust estimates of 3D reflector dip and azimuth. *Geophysics* **71**, P29–P40.

Marfurt K.J., Kirlin R.L., Farmer S.L. and Bahorich M.S. 1998. 3-D seismic attributes using a semblance-based coherency algorithm. *Geophysics* **63**, 1150–1165.

Sava P., Biondi B. and Etgen J. 2004. Diffraction-focusing migration velocity analysis, 74th SEG meeting, Denver, Colorado, USA, Expanded Abstracts, 2395–2399.

Schleicher J., Hubral P., Tygel M. and Jaya M.S. 1997. Minimum apertures and Fresnel zones in migration and demigration. *Geophysics* **62**, 183–194.

Shtivelman V. and Keydar S. 2004. Imaging shallow subsurface inhomogeneities by 3D multipath diffraction summation. *First Break* **23**, 39–42.

Taner M.T., Fomel S. and Landa E. 2006. Separation and imaging of seismic diffractions using plane-wave decomposition, 76th SEG meeting, New Orleans, Louisiana, USA, Expanded Abstracts, 2401.

Timoshin Y.V. 1978. *Seismic Pulse Holography*. Nedra (in Russian).

Tygel M., Schleicher J., Hubral P. and Hanitzsch C. 1993. Multiple weights in diffraction stack migration. *Geophysics* **59**, 1820–1830.